Forward and Reverse Shear Environments during Polar Low Genesis over the Northeast Atlantic

ANNICK TERPSTRA

Geophysical Institute, University of Bergen, Bergen, Norway

CLIO MICHEL AND THOMAS SPENGLER

Geophysical Institute, University of Bergen, and Bjerknes Centre for Climate Research, Bergen, Norway

(Manuscript received 9 September 2015, in final form 30 December 2015)

ABSTRACT

The synoptic and subsynoptic environments associated with polar low genesis are examined. Ambient pre–polar low environments are classified as forward or reverse shear conditions based on the angle between the thermal and mean wind. Forward shear environments are associated with a synoptic-scale ridge over Scandinavia, featuring a zonally oriented baroclinic zone extending throughout the troposphere with a wind speed maximum at the tropopause. Similar to typical midlatitude cyclogenesis, concurrent wavelike development occurs both in the lower and upper troposphere along the baroclinic zone and the mean propagation direction is eastward, parallel to isolines of sea surface temperature. Reverse shear environments exhibit a distinctly different structure and are characterized by a trough over Scandinavia, associated with a synoptic-scale, occluded cyclone. The genesis area exhibits strong cold air advection on its right-hand side and polar low development occurs on the warm side of an intense low-level jet. The environment resembles the characteristics conducive to secondary development associated with frontal instability. Polar lows developing in this configuration propagate mainly southward, perpendicular to isolines of sea surface temperature. The two genesis environments exhibit similar temperature differences between the sea surface and atmosphere near the surface, yet the magnitude of the surface fluxes is approximately double during reverse shear conditions due to stronger low-level winds. The ratio between surface sensible and latent heat fluxes is close to unity for both shear environments.

1. Introduction

Polar lows are intense, mesoscale cyclones developing over ice-free oceans at high latitudes (e.g., Rasmussen and Turner 2003). Previous climatologies of polar lows focused mainly on the large-scale atmospheric conditions associated with polar low events and thereby neglected subsynoptic features (e.g., Businger 1985; Claud et al. 2007; Blechschmidt et al. 2009; Mallet et al. 2013). However, given the relatively small length scale of polar lows, with a diameter between 200 and 700 km (Rasmussen and Turner 2003), the ambient subsynoptic environment arguably provides crucial links to the underlying dynamical mechanisms during development. In this study, we aim to fill this gap by identifying the synoptic and subsynoptic characteristics where we discriminate between two distinct subsynoptic environments associated with polar low genesis (i.e., forward and reverse shear).

Duncan (1978) defined reverse shear conditions as "a uniform, horizontal flow, in which the mean wind is parallel, but opposite in direction to the thermal wind," and elaborated that this condition can either be evaluated at a certain level or averaged over a layer. Utilizing a dry, linear, quasigeostrophic model, excluding surface friction and surface fluxes, Duncan (1978) showed that disturbances in reverse shear conditions are able to grow via baroclinic energy conversion. As the cold air is on the right side of the cyclone in these conditions, the warm (cold) air advection takes place in the rear (front) of the cyclone. The induced vertical motions and associated divergence fields exhibit a pattern that is reversed relative to the propagation of the cyclone when compared to the structure of usual extratropical cyclone growth (Fig. 1). Hence, Duncan (1978) coined this paradigm

Corresponding author address: Annick Terpstra, Geophysical Institute, University of Bergen, Postboks 7803, 5020 Bergen, Norway.
E-mail: annick.terpstra@gfi.uib.no

DOI: 10.1175/MWR-D-15-0314.1

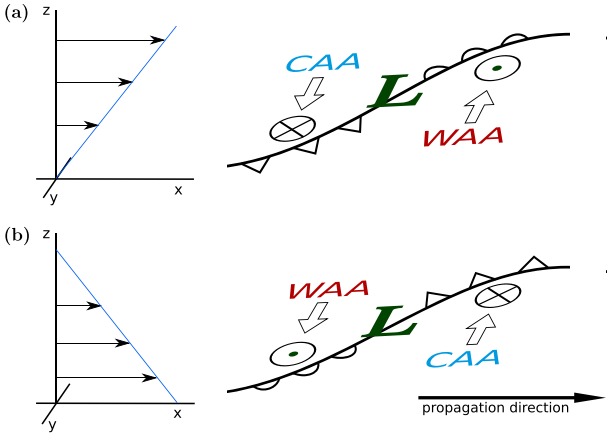

FIG. 1. Schematic of baroclinic cyclone development in (a) forward and (b) reverse shear environments. (left) Environmental vertical shear depicted by arrows representing wind. (right) Dry, idealized cyclone development. The lower-tropospheric frontal structures are depicted together with warm air advection (WAA) and cold air advection (CAA) (arrows) and approximate locations of maximum vertical motion (circles), with a dot indicating upward motion and a cross downward motion.

reverse shear. Note that reverse shear conditions refer to characteristics of the ambient cyclone environment and not to the polar low itself. As polar lows are generally warm-cored cyclones (e.g., Moore and Vonder Haar 2003), polar lows themselves will always be characterized by reverse shear.

Polar low development is usually preceded by a period of several days in which relatively cold and dry air, originating from ice-covered regions, is advected over the adjacent ice-free ocean (Businger 1985; Mallet et al. 2013). Noer et al. (2011) indicated that particularly the baroclinic periphery of these synoptic-scale cold air outbreaks is conducive for mesoscale cyclogenesis and indeed most polar lows studied developed along the outer edges of cold air outbreaks (e.g., Grønås et al. 1987; Reed and Duncan 1987; Nielsen 1997; Nordeng and Røsting 2011; Føre et al. 2011). During such cold air outbreaks, the penetrating cold air mass features a thermal wind direction opposite to the mean wind direction along its right-hand flank, thus leading to a reverse shear environment. In contrast, the left-hand flank of the cold air outbreak is characterized by forward shear conditions. Cold air outbreaks over the northeast Atlantic region exhibit both southward and eastward penetration directions, where the former is often confined by Greenland on its left-hand flank.

Although baroclinic cyclogenesis in reverse shear conditions is possible in a frictionless and dry atmosphere, Duncan (1978) also points out that the relatively strong low-level wind during reverse shear conditions potentially induces large surface fluxes and that friction might become important. Furthermore, his simplified model also excluded latent heating. The prominent role of diabatic heating during polar low development is evident in several numerical simulations of polar lows that all fail to develop when latent heating was switched off (e.g., Nordeng and Rasmussen 1992; Bresch et al. 1997; Nielsen 1997; McInnes et al. 2011). In addition, idealized simulations of polar low development indicate that the obtained growth rates are too small in the absence of diabatic heating (Craig and Cho 1988; Terpstra et al. 2015). Hence, the simplified model only partially captures the development of polar lows during reverse shear conditions. Therefore, other processes, especially related to diabatic effects, might play an important role during the development.

Even though baroclinicity is one of the primary ingredients for polar low genesis (Sardie and Warner 1983; Forbes and Lottes 1985; Nordeng 1987), the baroclinic structure of the atmosphere during polar low genesis is not necessarily similar for each polar low. Case studies indicate that the initial baroclinicity can extend throughout the entire depth of the atmosphere (e.g., Reed and Blier 1986; Hewson et al. 2000; Brümmer et al. 2009), whereas other polar lows originate in a low-level baroclinic zone associated with reverse shear conditions (e.g., Reed and Duncan 1987; Grønås et al. 1987; Bond and Shapiro 1991; Nordeng and Rasmussen 1992; Nielsen 1997; Føre et al. 2011). Analyzing developing and nondeveloping disturbances over the northeast Atlantic region, Forbes and Lottes (1985) point out that nearly 80% of the most intense disturbances developed during reverse shear conditions. However, as none of the previous studies addressed the different synoptic and subsynoptic characteristics of forward and reverse shear polar low environments, it is one of our main objectives to identify the atmospheric properties of forward and reverse shear conditions during polar low genesis.

The ensuing section introduces the dataset and polar low tracks used in our study. In section 3, we describe how we processed the polar low database as well as the reanalyses data, followed by section 4, where we present our results describing the environmental characteristics at polar low genesis time. Finally, section 5 recaps the main results and provides a short discussion about the implications of our results for future research on polar lows.

2. Data

a. *Polar low database*

We use the Sea Surface Temperature and Altimeter Synergy for Improved Forecasting of Polar Lows (STARS) database of polar lows, which is compiled to ''conduct a comprehensive scientific and technical review of polar lows in the Nordic Seas'' (Sætra et al.

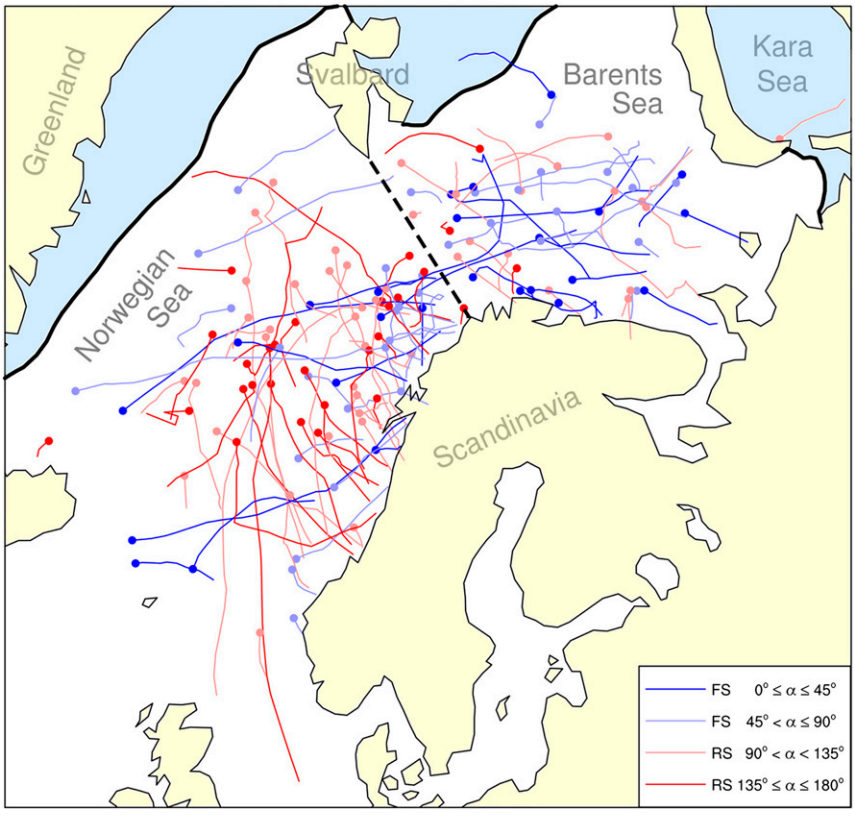

FIG. 2. Overview of the area of interest and the polar low tracks in the STARS database. The tracks are displayed as lines, with a solid circle at the genesis location. Dark and light blue tracks correspond to genesis environments classified as forward shear for $0° \le \alpha \le 45°$ and $45° < \alpha \le 90°$, respectively. Dark and light red tracks correspond to genesis environments classified as reverse shear for $135° \le \alpha \le 180°$ and $90° < \alpha < 135°$, respectively. The mean wintertime ice cover is shaded, and the dashed line is used as separation between the two ocean basins.

2010) and is freely available to the community (http://polarlow.met.no/). The database covers the period 2002–11, and contains a total of 140 polar low tracks in the northeast Atlantic area with hourly resolution. Identification and tracking of polar lows is based on manual inspection of operational weather forecasts and satellite products. In case of multiple polar low occurrences in close proximity of each other, the STARS database only records the track of the most intense polar low. For our study, we only consider tracks during the extended polar low season from October to April (Businger and Reed 1989) and discard polar low tracks consisting of only a single location. In addition, we discard one polar low due to its location north of Svalbard, as this area is usually covered with sea ice during the polar low season. We thus end up with a total of 131 polar lows for our analysis (Fig. 2).

b. *Atmospheric fields*

We use the European Centre for Medium-Range Weather Forecasts (ECMWF) interim reanalysis (ERA-Interim; Dee et al. 2011). The dataset is based on assimilating a wide range of observational data into the Integrated Forecast System (IFS) model with a four-dimensional variational data assimilation (4D-Var) analysis method. Hence, it can be regarded as a close-to-observation representation of the full three-dimensional state of the atmosphere. The data have a 6-h time resolution and our analysis is based on a version interpolated onto a horizontal grid of $0.5° \times 0.5°$.

Previous studies indicated that the structures associated with polar lows are generally too weak (Condron et al. 2006; Laffineur et al. 2014; Zappa et al. 2014) and not all observed polar lows are present in the ERA-Interim dataset. For example, Zappa et al. (2014) used an automatic tracking scheme and only detected 55% of the polar lows from the STARS database in ERA-Interim. However, our goal is not to track polar lows, but to identify the ambient pre–polar low environment. As the typical horizontal length scales of pre–polar low environments are determined by the (sub)synoptic-scale configuration, we do not expect the accuracy of the representation of polar

lows themselves in ERA-Interim to significantly impact our results. Thus, the resolution of ERA-Interim should be sufficient for our analysis.

3. Method

a. *Definition of the ambient pre–polar low environment*

We define the first location of a polar low track in the STARS database as the *genesis location*. However, as the genesis location in the STARS database is derived from satellite products, the polar low must have already developed a distinctive cloud structure. Assuming a typical spinup time for polar lows of about up to 12 h, we examine the pertinent ERA-Interim fields 7–12 h prior to the STARS genesis time to obtain the typical atmospheric environment in which polar lows form. The chosen time window allows us to uniquely identify a time step in the 6-hourly ERA-Interim data prior to the time of first occurrence in the STARS database. Subsequently, we will refer to this ERA-Interim time step as *genesis time*.

b. *Propagation direction, rotation of ERA-Interim data, and composites*

We define the direction of propagation as the angle between the great circle linking the first and last location of the polar low track and geographic North. The mean propagation speed of each polar low is determined by the lifetime of the polar low divided by the length of the great circle linking the first and last point of the STARS track. Contrary to the relative zonal propagation direction of extratropical cyclones, we found that polar lows do not exhibit a common propagation direction. Therefore, we rotate the ERA-Interim fields such that the polar low propagation is "eastward." This allows for a direct comparison of the respective ambient conditions of polar low genesis relative to the direction of propagation. We consider ERA-Interim data centered at the genesis location and interpolate the rotated data to a regularly spaced grid with a grid spacing of 25 km.

Rotated ERA-Interim fields are used to composite the polar low relative environment, whereas we use unrotated ERA-Interim data to illustrate the synoptic-scale environment and calculate confidence intervals for anomalies utilizing a bootstrap (Wilks 2006) method with respect to wintertime (October–April) mean values.

c. *Shear criterion*

Given the definition of reverse shear (Duncan 1978), a key parameter to distinguish between different polar low environments is the angle between the thermal wind and the mean flow in the lower troposphere, where the thermal wind is aligned (opposite) with the steering-level flow for forward (reverse) shear polar lows. We will use this angle between the mean and thermal wind to distinguish between forward and reverse shear polar lows from the STARS database and perform a composite analysis to highlight the differences between forward and reverse shear polar low genesis environments.

To determine the aforementioned angle, we calculate the thermal wind $\mathbf{v}_T = (u_T, v_T)$ between 925 and 700 hPa:

$$u_T = -\frac{1}{f}\frac{\partial(\phi_{700} - \phi_{925})}{a\partial\varphi} \quad \text{and} \quad v_T = \frac{1}{f}\frac{\partial(\phi_{700} - \phi_{925})}{a\cos\varphi\partial\lambda}, \tag{1}$$

where u_T and v_T are the components of the thermal wind; f is the Coriolis parameter; φ and λ are the latitude and longitude, respectively; a represents the radius of the earth; and ϕ_{700} and ϕ_{925} are the geopotential at 700 and 925 hPa, respectively. We define the mean wind $\overline{\mathbf{v}} = (\overline{u}, \overline{v})$ as the vertically averaged wind between 925 and 700 hPa. The angle α between the mean and thermal wind,

$$\alpha = \arccos\left(\frac{\mathbf{v}_T \cdot \overline{\mathbf{v}}}{\|\mathbf{v}_T\|\|\overline{\mathbf{v}}\|}\right), \tag{2}$$

is then used to distinguish between forward and reverse shear. Following Kolstad (2006), we classify pre–polar low conditions with $0° \le \alpha \le 45°$ as forward shear and conditions with $135° \le \alpha \le 180°$ as reverse shear. Forbes and Lottes (1985) used $90° \le \alpha \le 180°$ to define reverse shear conditions. Application of these less restricted criteria to our analysis yields similar results, though with a slightly weaker amplitude (not shown).

Kolstad (2006) used a steering-level wind at either 775 or 850 hPa instead of the mean wind. Applying both of his steering levels to the STARS dataset, it turns out that the 775-hPa level is redundant; that is, polar low environments classified as reverse shear using the 775-hPa wind are a subset of the polar low environments classified as reverse shear when using the 850-hPa wind.

As surface friction decreases wind speed in the very lowest part of the troposphere, the 925-hPa level is a reasonable choice as lower bound because it is not affected too much by the boundary layer. Furthermore, increasing the upper bound up to 500 hPa did not significantly change the results (not shown), indicating that the 925–700-hPa shear conditions are representative for the troposphere.

To identify the different environments in which polar lows develop, we average the shear criterion over a radius of 200 km around the genesis location at the genesis

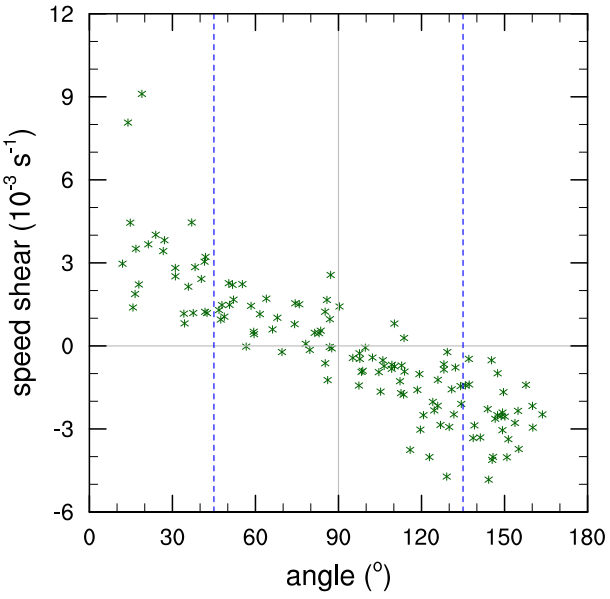

FIG. 3. Vertical gradient of total wind speed between 925 and 700 hPa (10^{-3} s^{-1}) vs the angle between the thermal and mean wind between 925 and 700 hPa (°). Dashed lines indicate the angle limits for reverse (135°) and forward (45°) shear.

time for all polar lows. Given that the average diameter of polar lows is ~300 km (Condron et al. 2006), a 200-km radius is assumed to be representative for their genesis area. Sensitivity tests of the applied radius indicate that increasing the radius resulted in a reduction of polar low environments classified as reverse/forward shear, which is in agreement with the relatively narrow flanks of cold air outbreaks.

4. Results

a. Shear criterion

The angle between the thermal wind and the mean wind in pre–polar low environments is related to the vertical gradient of total wind speed within the same layer (Fig. 3). Angles greater than 90° correspond roughly to a wind speed decreasing with height, whereas angles less than 90° correspond to a wind speed increasing with height. Furthermore, the angles are nearly equally distributed from 0° to 180°, indicating that there is no clear preference with respect to environmental shear for polar low development.

Using our shear criterion, 28 (25) polar lows developed in a reverse (forward) shear environment.[1] Hence, about 21% (19%) of polar lows in the STARS database developed in reverse (forward) shear conditions. Applying the same criteria, Blechschmidt (2008) identified 22% of the polar lows in their database developing in reverse shear conditions. Using $90° \leq \alpha \leq 180°$ to classify reverse shear conditions, Forbes and Lottes (1985) identified 66% of their environments as reverse shear, whereas for the STARS database 55% of the polar lows would fulfil this criterion. Overall, the percentage of polar lows developing in reverse shear conditions agrees well with other polar low databases.

Among all considered polar low tracks, six tracks were associated with multiple polar low occurrences, of these three (one) were classified as reverse (forward) shear. Because of the relative rare occurrence of multiple polar lows in the STARS database, they most likely do not significantly impact our results.

b. Synoptic-scale configuration and propagation direction

The synoptic-scale configuration during forward shear conditions is characterized by a significant dipole in both the 850-hPa temperature field and the 500-hPa geopotential height (Figs. 4a,b). Compared to wintertime mean values, relatively warm 850-hPa temperatures and high 500-hPa geopotential heights are located over southern Scandinavia, whereas relatively cold 850-hPa temperatures and low 500-hPa geopotential heights are located on the northern side of the Barents Sea. This configuration corresponds to a ridge extending far into the Nordic Seas. In the lower troposphere, a broad, zonally oriented baroclinic zone is evident, manifested in the north–south temperature gradient covering both the Barents and Norwegian Seas (Fig. 4b). Similarly, strong north–south temperature gradients are located at the tropopause (Fig. 4a) over the Norwegian Sea (~65°N) and over the Barents Sea. This upper-level temperature gradient indicates a sloping tropopause and is associated with enhanced zonal wind speeds at this level. Hence, forward shear conditions feature a zonally oriented baroclinic zone located over the Norwegian and Barents Seas (Figs. 4a,b) extending throughout the whole depth of the troposphere.

The synoptic pattern associated with reverse shear polar lows consists of significantly high 850-hPa temperature and 500-hPa geopotential height over the entire Nordic Seas area (Figs. 4c,d), constituting a synoptic-scale trough over Scandinavia. Over the Barents Sea, the uniform geopotential height at 500 hPa and very weak temperature gradients at the tropopause indicate that the upper troposphere is practically barotropic (Fig. 4c). A north–south-oriented temperature gradient at the tropopause

[1] STARS track identifier for reverse (forward) shear environments: 5, 8, 9, 15, 20, 26, 27, 29, 36, 42, 43, 71, 79, 82, 91, 92, 93, 94, 96, 98, 101, 103, 111, 112, 121, 126, 129, and 134 (2, 3, 21, 22, 25, 41, 50, 51, 52, 54, 55, 63, 65, 73, 75, 95, 99, 106, 115, 119, 120, 130, 132, 133, and 140).

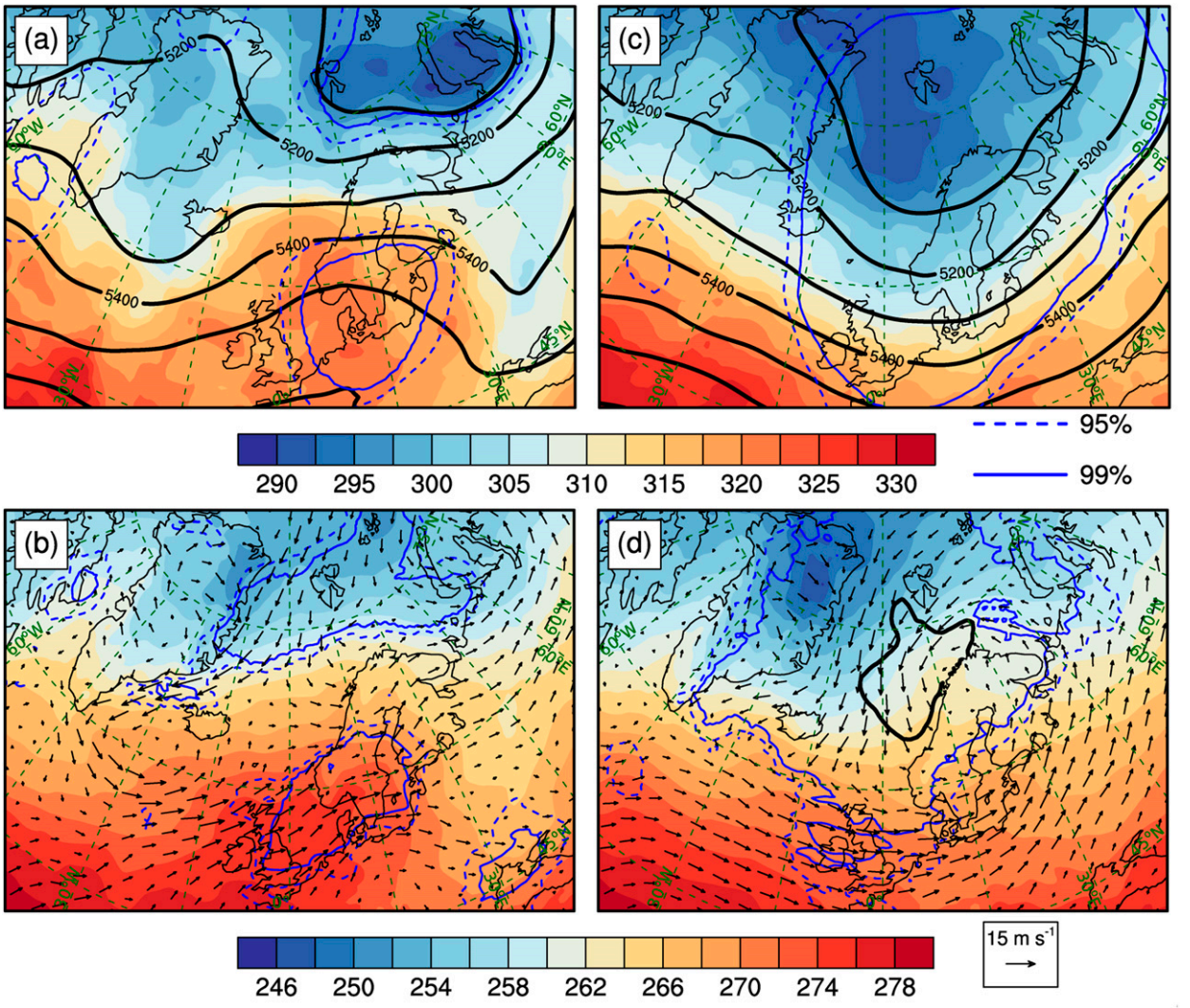

FIG. 4. (top) Composites of the geopotential height at 500 hPa (m; black solid lines), potential temperature on the 2-PVU surface (K; shading), and the 95% and 99% confidence levels calculated for the 500-hPa geopotential (blue dashed and solid lines, respectively). (bottom) Composites of the horizontal wind (arrows) and temperature at 850 hPa (K; shading), difference between SST and temperature at 500 hPa (K; black line representing the 43-K contour, threshold not reached during forward shear conditions), and the 95% and 99% confidence levels calculated for the 850-hPa temperature (blue dashed and solid lines, respectively). (a),(b) Composites for forward and (c),(d) reverse shear conditions. Confidence intervals are with respect to the differences from the mean wintertime values.

is present over the Norwegian Sea (~68°N). However, this temperature gradient is weaker than for forward shear conditions. The lower troposphere is characterized by a strong cold air outbreak, where the coldest air and strongest low-level winds are located in the western Norwegian Sea (Fig. 4d). The resulting pattern is a northwest–southeast-oriented temperature gradient, roughly perpendicular to the Norwegian coast. Thus, reverse shear conditions are characterized by a low-level baroclinic zone on the eastern flank of a cold air outbreak, and a nearly barotropic upper troposphere above the genesis area.

Both forward and reverse shear conditions are characterized by a cold air outbreak, indicated by the southward low-level flow off the ice-covered region and the relatively cold temperatures over the northern part of the Nordic Seas (Figs. 4b,d). However, during reverse shear conditions the cold air outbreak features stronger low-level winds and colder temperatures. Furthermore, in the case of reverse shear conditions, the cold air penetrates farther south and covers the western part of the Norwegian Sea.

Polar lows developing in forward shear environments tend to propagate in an eastward direction, whereas polar lows developing in reverse shear environments

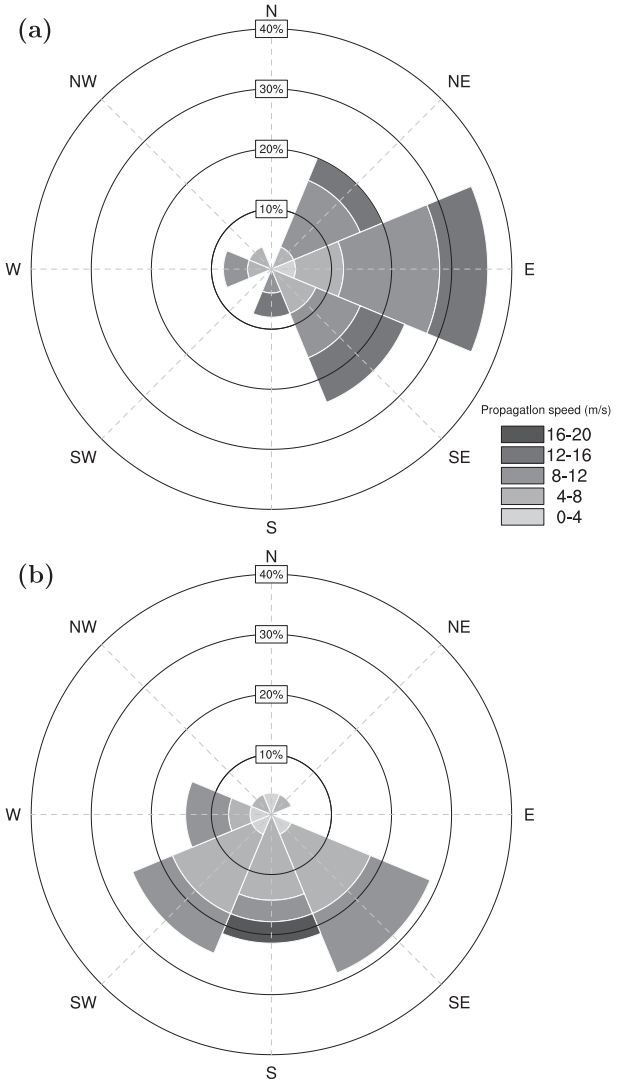

FIG. 5. Propagation characteristics for (a) forward and (b) reverse shear conditions. The gray shading represents the propagation speed ($m\,s^{-1}$) and the circles represent the frequencies of the directions (%).

exhibit a southward propagation direction (Fig. 5). As the mean flow mainly determines the propagation direction of embedded cyclones, this distinct difference in propagation direction is linked to the synoptic-scale flow patterns associated with the two different shear environments. Forward shear polar lows tend to develop along the zonally oriented baroclinic zone between Greenland and the Kara Sea and were found both in the Norwegian Sea and Barents Sea regions (Fig. 2). As reverse shear polar lows tend to propagate southward, one would expect them to occur more often in the Norwegian Sea, although several reverse shear polar lows occurred in the Barents Sea region. Bracegirdle and Gray (2008) noticed that a southward mean flow direction during polar low development occurs only 58% of the time, which agrees well with the percentage of polar lows in the STARS database within $90° \leq \alpha \leq 180°$ (i.e., the extended range for the definition of reverse shear polar lows).

To address the spatial distribution of forward and reverse shear environments, we focus on the development over the two major ocean basins in the area: the Norwegian Sea and the Barents Sea (Fig. 2). Out of all examined polar low tracks, 37% of the polar lows occurred over the Barents Sea, and 63% occurred over the Norwegian Sea. For environments classified as forward shear, 44% occurred over the Norwegian Sea, whereas 56% occurred over the Barents Sea. Hence, the distribution of forward shear environments is rather similar to the distribution of all polar lows, indicating that forward shear environments are found in both regions. In contrast, for reverse shear conditions, 85% occur over the Norwegian Sea versus 15% over the Barents Sea. Thus, there appears to be a tendency for reverse shear conditions to occur more often over the Norwegian Sea.

The temperature difference between the sea surface temperature (SST) and the temperature at 500 hPa T_{500} is often used as a proxy for potential polar low development (e.g., Rasmussen and Turner 2003). In this study, we averaged the SST $-$ T_{500} difference in the 200-km radius around the genesis location at the genesis time. During reverse shear conditions, the synoptic-scale trough and the associated lowering of the tropopause over the Norwegian Sea results in a larger temperature difference between the SST and 500-hPa temperature (45.2 ± 2.6 K) than for forward shear conditions (41.0 ± 3.6 K). Typical values for the SST $-$ T_{500} difference during polar low development over the Atlantic basin range between 36 and 52 K (Blechschmidt et al. 2009), with average values around 45–46 K (Blechschmidt et al. 2009; Laffineur et al. 2014). The SST $-$ T_{500} differences for all polar low genesis environments in the STARS database range between 33 and 53 K with an average of 44.0 ± 3.6 K, which is in agreement with the previously mentioned studies.

c. *Subsynoptic environment for forward and reverse shear conditions*

1) VERTICAL PROFILES

To identify the characteristics of the subsynoptic pre–polar low environments in terms of static stability, relative humidity, and wind, we calculated the area-averaged vertical profiles of the rotated fields in a 200-km radius around all 131 polar low genesis locations at genesis time. Comparing the mean wind speed in

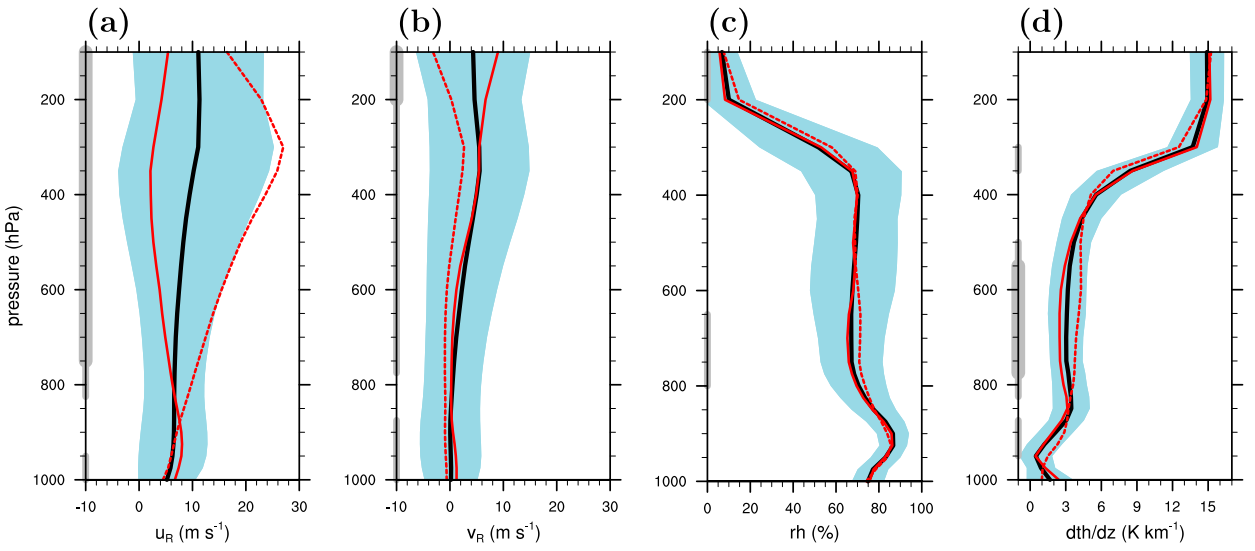

FIG. 6. Area-averaged (r = 200 km) vertical profiles at the genesis location for (a) wind in the propagation direction (i.e., u_R; m s^{-1}), (b) wind in the orthogonal direction of the propagation direction (i.e., v_R; m s^{-1}), (c) relative humidity (%), and (d) vertical stratification (i.e., $d\theta/dz$; K km^{-1}). The black line corresponds to the mean for all polar lows whereas the shading corresponds to one std dev around the mean. The solid and dashed red lines are the averages for reverse and forward shear cases, respectively. Shading on vertical axes indicate levels with statistical significant differences between forward and reverse shear (significance level = 0.05), thick shading Cohen's $d > 0.8$.

the direction of propagation u_R profiles for forward and reverse shear conditions to the total mean, it is evident that the standard deviation for all cases reflects the two ends of the spectrum of environmental conditions (Fig. 6a). Thus, u_R for all polar lows (black line) is approximately the average of u_R for the forward (dashed red line) and reverse (solid red line) conditions. Note that u_R is positive for both shear conditions, though it increases with height for forward shear conditions and decreases with height for reverse shear conditions.

The wind speed perpendicular to the propagation direction v_R is close to zero throughout the depth of the troposphere for forward shear conditions, but exhibits a slight increase with height during reverse shear conditions (Fig. 6b).

Relative humidity profiles are similar for both reverse and forward shear conditions (Fig. 6c), with surface relative humidities around 75% increasing within the boundary layer to ~85% and decreasing above to ~60%. A sharp decrease in relative humidity is located at the tropopause around 400 hPa.

The vertical stratification $d\theta/dz$ (where θ is the potential temperature and z is the height) for reverse shear conditions is characterized by a strong boundary layer inversion between 950 and 850 hPa, whereas this inversion is less pronounced for forward shear conditions (Fig. 6d). Throughout the rest of the troposphere, forward shear conditions are more stratified than reverse shear conditions and the tropopause, evident by a strong inversion, is located at elevated pressure levels for forward shear conditions. The lowered tropopause and reduced stratification during reverse shear conditions are consistent with the relatively cold temperatures at the tropopause (i.e., lower tropopause heights over the Nordic Seas region; Fig. 4c).

We used a Student's t test (Wilks 2006) to evaluate the null hypothesis that the sample means for forward and reverse are from the same population. The difference in vertical stability at midtropospheric levels between forward and reverse shear conditions is statistically significant (significance level = 0.05; Fig. 6d). However, in order to address the dynamical relevance, for example, the potential for deep convection, one needs to take into account both the strength of the inversion capping the boundary layer and the stability in the midtroposphere, as opposed to considering a level-by-level-based statistical significance. Similarly, the difference in wind speed in the direction of propagation (u_R) is not statistically significant in the lower atmosphere (Fig. 6a), though the opposite signs of vertical shear for forward and reverse shear conditions have significant dynamical ramifications.

2) HORIZONTAL FIELDS

To further characterize the subsynoptic reverse and forward shear environments, we examined composites of rotated atmospheric fields around the genesis location for each shear condition. All fields are rotated such that the direction of propagation is toward the east and the following nomenclature is adopted to describe the

relative location with respect to the genesis location, which is located in the center of each figure: locations ahead and in the wake of the propagating cyclone are referred to as front and rear of the genesis area, respectively, and left and right are used with respect to the propagation direction. The rotated fields are examined at the genesis time and 12 h prior and after. Because of the rotated framework, areas over land or ice are present in the periphery of the composites. Therefore, we masked areas in the surface variable composites where the polar low genesis environments were above land or ice for more than 75% of the cases.

Note that, especially in Arctic regions, the presence of a potential temperature anomaly at the tropopause is distinctly different from a potential vorticity (PV) anomaly at 300 hPa, the latter being used in climatological studies (e.g., Mallet et al. 2013) to identify upper-level PV anomalies associated with polar lows. However, for the reverse shear conditions the 300-hPa level is located entirely in the stratosphere, hence an anomaly in the PV field at 300 hPa would not necessarily represent a downward tropopause fold, and can easily be relatively large due to high PV values and large vertical PV gradients in the stratosphere. Therefore, we use the potential temperature at the dynamical tropopause, defined by the 2-PVU (potential vorticity unit) ($1\,\mathrm{PVU} = 10^{-6}\,\mathrm{K\,kg^{-1}\,m^2\,s^{-1}}$) isosurface, to indicate upper-level anomalies in the ambient polar low environments.

Forward shear conditions are characterized by the alignment of the 500-hPa geopotential height and the 850-hPa potential temperature contours with the direction of propagation (Figs. 7a–c). A small-scale wave in the 850-hPa temperature develops roughly at the genesis location and propagates eastward (Figs. 7a–c). At genesis time ($t = 0$; Fig. 7b) a potential temperature anomaly at the tropopause is positioned at the left-rear side of the genesis location indicating a localized lowering of the tropopause. As the polar low develops, this upper-level feature intensifies and migrates eastward. Hence, the alignment of the upper- and lower-level baroclinic zone and the simultaneous wavelike growth in the upper and lower troposphere indicate that polar low development during forward shear conditions is similar to typical midlatitude baroclinic development (e.g., Dacre et al. 2012).

The reverse shear environment exhibits distinctly different features, with a warm tongue in the 850-hPa temperature field on the left side of the genesis location and a minimum in 500-hPa geopotential height above the genesis location (Fig. 7e). These features indicate that an old, occluded synoptic low is situated over the genesis location. This configuration exhibits strong cold air advection on the right side of the genesis location. Compared to the forward shear conditions, the low-level baroclinic zone, evident in the 850-hPa temperature field, is oriented more perpendicular to the propagation direction. At the genesis time, an upper-level potential temperature perturbation develops over the genesis location, expanding horizontally over time (Figs. 7d–f).

The reverse shear composite shows striking similarity with the conceptual drawing in Bond and Shapiro (1991) (see their Fig. 20) of a reverse shear polar low. Similar to other reverse shear polar low cases (e.g., Grønås et al. 1987; Reed and Duncan 1987; Nielsen 1997), this polar low developed in a tongue of warm air in the form of a bent-back occlusion on the western side of a synoptic-scale cyclone. Furthermore, the associated low-level baroclinic zone was enhanced by differential cold air advection. Reed and Duncan (1987) also noted weak gradients in the geopotential height at 500 hPa. Hence, the reverse shear composites are in good agreement with observed reverse shear polar lows.

3) Vertical cross sections

A vertical left–right cross section of the forward shear composites at the genesis location shows a baroclinic zone extending throughout the entire depth of the troposphere (Fig. 8a), evident from the sloping isentropes (black lines) and sloping tropopause (gray line). The cold air is located on the left side of the genesis location and the jet maximum is located at the tropopause height on the right-hand side of the genesis location.

In a similar cross section for reverse shear conditions, the wind field features a quasi-barotropic synoptic-scale trough centered around the genesis location, evident in the positive and negative wind distribution at upper levels perpendicular to the cross section and the relatively flat tropopause (Fig. 8b). The most striking difference compared to forward shear conditions is the prominent low-level jet and its associated baroclinic zone located to the right of the genesis location. The upward bulging isentropes above the low-level jet are associated with cold air advection on the right-hand side of the genesis location (Fig. 8b). Note that the genesis location is on the warm side of the low-level baroclinic zone for both shear conditions.

Aircraft observations of pre–polar low environments are rare and we are only aware of one flight mission targeting the incipient polar low environment. This polar low developed in a typical reverse shear environment and two flight legs were roughly perpendicular to the direction of the propagation of the polar low [see Fig. 7 in Føre et al. (2011) and Fig. 8 in Kristjánsson et al. (2011)]. Similar to our composite (Fig. 8b), the observations indicate a strong low-level jet located on

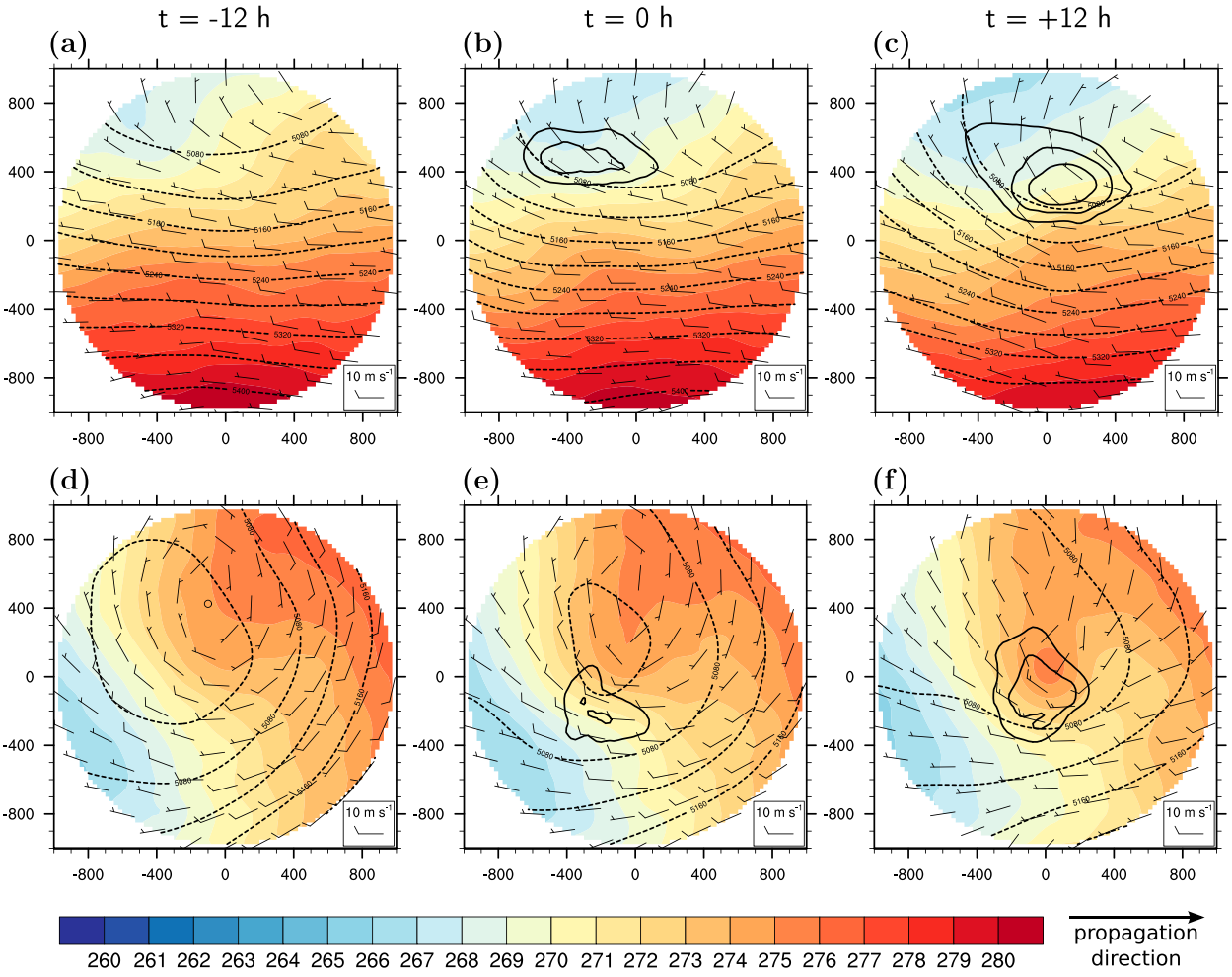

FIG. 7. Horizontal composites in the rotated frame for (a)–(c) forward and (d)–(f) reverse shear conditions of the potential temperature at 850 hPa (K; shading), wind at 850 hPa (wind barbs), geopotential height at 500 hPa (m; dashed lines), and potential temperature at 2 PVU (K; solid line, first contour is 291 K and contour interval is 1 K). Results are (left) 12 h before the genesis time ($t = -12$ h), (center) at the genesis time ($t = 0$ h), and (right) 12 h after the genesis time ($t = 12$ h). Values on the axes indicate the distance (km) from the genesis location.

the cold side of the low-level baroclinic zone. However, the intensity of the observed low-level jet is almost 3 times as strong as in the composite, which is somewhat expected due to the coarse resolution of ERA-Interim and the smoother nature of composites. Still, the similarities indicate that the structures of the reverse shear composite are in general agreement with these observations.

4) SURFACE CHARACTERISTICS

Polar lows propagate along the SST isolines in forward shear conditions (Fig. 9a), whereas they propagate in the perpendicular direction toward warmer SSTs during reverse shear conditions (Fig. 9b). Similarities between the SST pattern (Fig. 9) and the 850-hPa temperature field (Figs. 7b,e) indicate the prominent role of the SSTs in setting up the lower-tropospheric baroclinic zone. Reverse shear polar lows develop over areas with higher SSTs, but the difference between the SST and the 2-m temperature at the genesis location is similar (around 6–7 K) for both shear conditions (Fig. 9). The difference between SST and 2-m temperature is largest on the left-hand side for forward shear conditions, and on the rear and right-hand side for reverse shear conditions.

Neglecting the influence of wind, one would expect the largest sensible heat fluxes in areas of strong temperature contrast, which is indeed the case. However, due to the stronger low-level jet for reverse shear cases, surface fluxes are enhanced for reverse compared to forward shear conditions (Fig. 10). The ratio between latent and sensible heat fluxes is close to unity for both

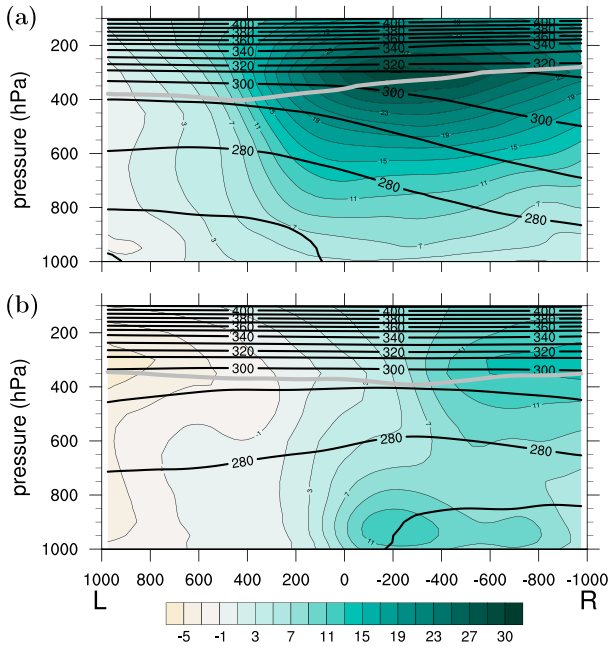

FIG. 8. Vertical cross sections of composites in the rotated frame of the wind in the propagation direction ($m\,s^{-1}$), potential temperature (K; solid lines), and dynamic tropopause defined by the 2-PVU surface (solid gray line) for (a) forward and (b) reverse shear conditions from the left (L) to the right (R) of the propagation direction. Values on the horizontal axis indicate the distance (km) from the genesis location.

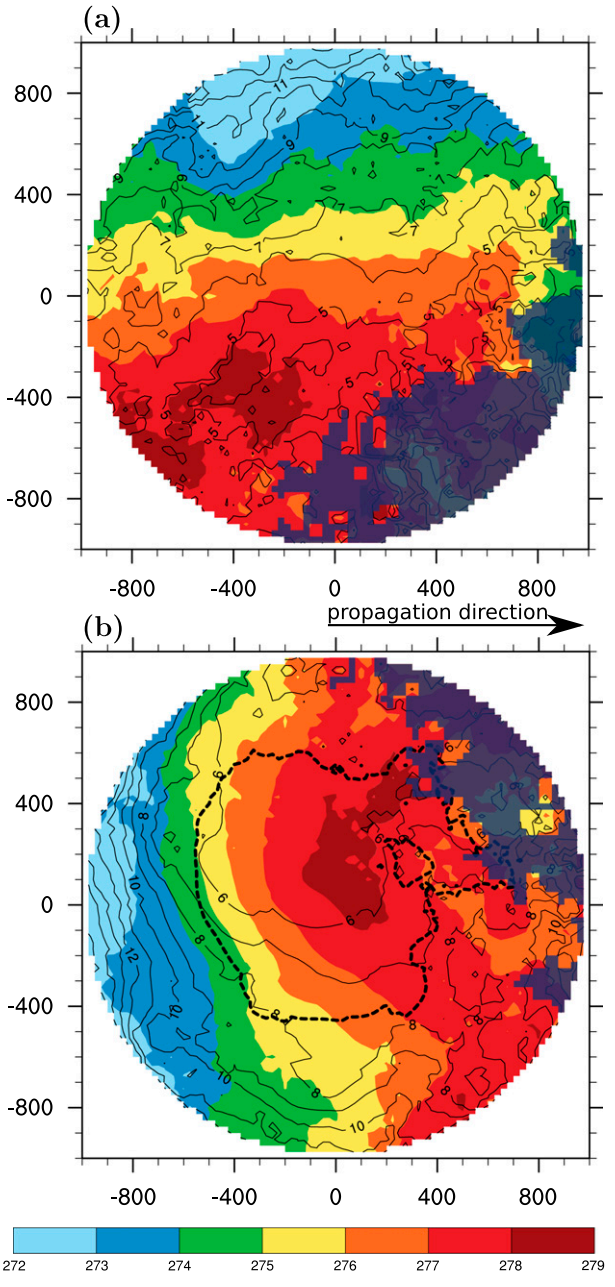

FIG. 9. Composites in the rotated frame of SST (K; shading), temperature difference between SST and 2-m temperature (K; solid lines), and temperature difference between SST and temperature at 500 hPa (K; dashed line representing the 43-K contour, threshold not reached during forward shear conditions) for (a) forward and (b) reverse shear conditions. Areas with less than 75% of ocean are masked. Values on the axes indicate the distance (km) from the genesis location.

reverse and forward shear conditions, but the magnitude of the fluxes for reverse shear conditions ($\sim$140 $W\,m^{-2}$) is approximately doubled compared to forward shear conditions ($\sim$70 $W\,m^{-2}$). Therefore, as the differences between the SST and 2-m temperature are similar, this difference in magnitude in fluxes can be mainly attributed to stronger low-level wind during reverse shear conditions, where the region of enhanced surface fluxes is collocated with the position of the low-level jet.

5. Discussion and conclusions

We provided an overview of the ambient atmospheric conditions during polar low genesis, where we determined the angle between the thermal wind and the mean flow in the lower troposphere in the subsynoptic polar low genesis environment to identify two distinctly different environments in which polar low genesis takes place; namely, forward and reverse shear conditions. Our reverse shear composites are in agreement with observations and case studies, confirming that our method is successful in discriminating between forward and reverse shear environments.

The forward shear environment is similar to environments typical for midlatitude cyclogenesis and is characterized by a baroclinic jet extending throughout the entire depth of the troposphere with a wind speed maximum at the tropopause. The synoptic-scale pattern is characterized by a zonally oriented baroclinic zone associated with a ridge over Scandinavia and the propagation direction of

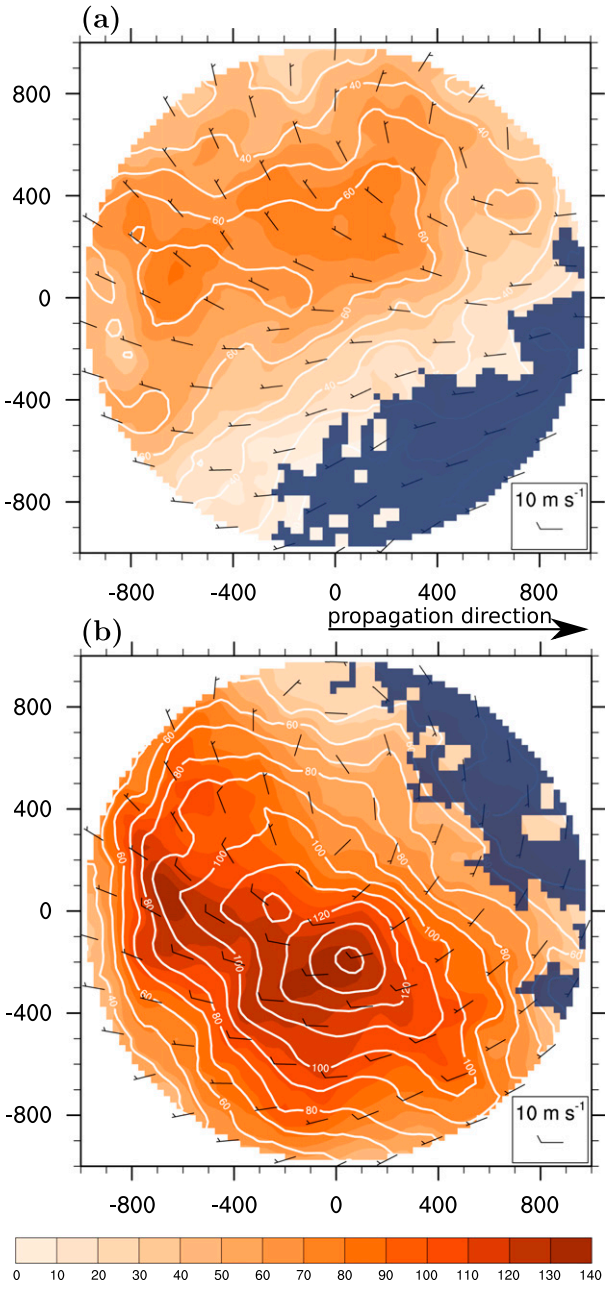

FIG. 10. Composites in the rotated frame of the surface sensible heat flux ($W m^{-2}$; shading), latent heat flux ($W m^{-2}$; solid lines), and wind at 10 m (wind barbs) for (a) forward and (b) reverse shear conditions. Areas with less than 75% of ocean are masked. Values on the axes indicate the distance (km) from the genesis location.

these polar lows is mainly eastward along this baroclinic zone. Furthermore, the surface fluxes exhibit moderate strength and the propagation direction of polar lows is along SST isolines.

The synoptic-scale configuration during reverse shear conditions is characterized by a trough over Scandinavia associated with a synoptic-scale, occluded cyclone. The genesis area exhibits cold air advection on the right-hand side and polar low development takes place on the warm side of a strong low-level baroclinic zone with an intense low-level jet. The SSTs are similar for both shear conditions, but reverse shear conditions are associated with larger temperature differences between SST and temperature at 500 hPa. Reverse shear polar lows are associated with average values for the SST $-$ T_{500} difference greater than 43 K, whereas this threshold is not reached during forward shear conditions (Fig. 9d). However, recent climatologies of polar lows adopted a stringent criterion, SST $-$ $T_{500} > 43$ K, to identify polar lows (Zahn and von Storch 2008; Zahn et al. 2008; Zahn and von Storch 2010; Zappa et al. 2014), and thereby potentially excluded forward shear polar lows. In addition, Zahn and von Storch (2008), Zahn et al. (2008), and Zahn and von Storch (2010) required a southward component in the propagation direction for polar lows, thereby further limiting their ability to identify polar lows that develop during forward shear conditions.

Because of the low-level jet, surface fluxes during polar low genesis are twice as intense for reverse shear environments compared to forward shear environments. Furthermore, reverse shear polar lows tend to propagate southward and toward the warm side of the SST field.

Contrary to most previous climatologies of polar lows, we stratified the polar low database based on a dynamical argument (i.e., differences in lower-tropospheric shear) instead of using a spatial separation or large-scale weather patterns. The separation between forward and reverse shear environments by applying the shear criterion agrees to some extent with previous descriptive identification methods for polar low types. Businger and Reed (1989) distinguished between the shortwave/jet-streak type and the Arctic front type where they associated the latter with reverse shear polar lows and the former with forward shear polar lows. Our method of separation provides a more stringent identification of the conditions in which polar lows develop. Knowledge of these conditions can serve as a starting point for the investigation of the dynamical mechanisms underlying the different types of polar low development. Furthermore, this knowledge potentially aids forecasting of polar lows by identifying environments conducive for certain types of polar low development and could be used to identify if certain polar low types are more predictable than others.

To underline the notion that forward and reverse shear are two distinctly different environments, we deliberately chose to examine the ends of the spectrum of genesis environments by applying a more restrictive criteria. However, when we divided the dataset in two categories separated by $\alpha = 90°$, the results exhibit

similar environmental characteristics, though with slightly less pronounced features.

Despite the common occurrence of reverse shear conditions during polar low development, relatively little attention has been given to the dynamical relevance of the atmospheric configuration during reverse shear condition. It is, thus, not surprising that the low-level jet and frontal structure were not included in the reverse shear paradigm proposed by Duncan (1978). However, based on our analysis, we firmly believe that these features are essential and cannot be neglected when addressing reverse shear polar low genesis. In fact, these features closely resemble the environment for secondary development associated with frontal instability (Schär and Davies 1990; Joly and Thorpe 1990), which we hypothesize to be the most likely dynamical pathway underlying polar low genesis during reverse shear conditions.

Furthermore, our analysis indicates that reverse shear polar lows are associated with stronger surface heat and moisture fluxes and that they grow in a slightly less stratified troposphere compared to forward shear conditions. Both features indicate that reverse shear polar low environments might be more conducive to initiate convection. However, both the initiation of convection and the role of the low-level jet in their development need to be further clarified with respect to polar low development in reverse shear conditions.

Acknowledgments. We thank ECMWF for providing the ERA-Interim data used within this study, and the Norwegian Meteorological Institute for providing the STARS polar low database. This work is supported by the Norwegian Research Council as part of High Impact Weather in the Arctic (Project 207875). We thank two anonymous reviewers for their valuable comments.

REFERENCES

Blechschmidt, A.-M., 2008: A 2-year climatology of polar low events over the Nordic Seas from satellite remote sensing. *Geophys. Res. Lett.*, **35**, L09815, doi:10.1029/2008GL033706.

——, S. Bakan, and H. Graßl, 2009: Large-scale atmospheric circulation patterns during polar low events over the Nordic Seas. *J. Geophys. Res.*, **114**, D06115, doi:10.1029/2008JD010865.

Bond, N. A., and M. Shapiro, 1991: Polar lows over the Gulf of Alaska in conditions of reverse shear. *Mon. Wea. Rev.*, **119**, 551–572, doi:10.1175/1520-0493(1991)119<0551:PLOTGO>2.0.CO;2.

Bracegirdle, T. J., and S. L. Gray, 2008: An objective climatology of the dynamical forcing of polar lows in the Nordic Seas. *Int. J. Climatol.*, **28**, 1903–1919, doi:10.1002/joc.1686.

Bresch, J. F., R. J. Reed, and M. D. Albright, 1997: A polar-low development over the Bering Sea: Analysis, numerical simulation, and sensitivity experiments. *Mon. Wea. Rev.*, **125**, 3109–3130, doi:10.1175/1520-0493(1997)125<3109:APLDOT>2.0.CO;2.

Brümmer, B., G. Müller, and G. Noer, 2009: A polar low pair over the Norwegian Sea. *Mon. Wea. Rev.*, **137**, 2559–2575, doi:10.1175/2009MWR2864.1.

Businger, S., 1985: The synoptic climatology of polar low outbreaks. *Tellus*, **37A**, 419–432, doi:10.1111/j.1600-0870.1985.tb00441.x.

——, and R. J. Reed, 1989: Cyclogenesis in cold air masses. *Wea. Forecasting*, **4**, 133–156, doi:10.1175/1520-0434(1989)004<0133:CICAM>2.0.CO;2.

Claud, C., B. Duchiron, and P. Terray, 2007: Associations between large-scale atmospheric circulation and polar low developments over the North Atlantic during winter. *J. Geophys. Res.*, **112**, D12101, doi:10.1029/2006JD008251.

Condron, A., G. R. Bigg, and I. A. Renfrew, 2006: Polar mesoscale cyclones in the Northeast Atlantic: Comparing climatologies from ERA-40 and satellite imagery. *Mon. Wea. Rev.*, **134**, 1518–1533, doi:10.1175/MWR3136.1.

Craig, G., and H.-R. Cho, 1988: Cumulus heating and CISK in the extratropical atmosphere. Part I: Polar lows and comma clouds. *J. Atmos. Sci.*, **45**, 2622–2640, doi:10.1175/1520-0469(1988)045<2622:CHACIT>2.0.CO;2.

Dacre, H., M. Hawcroft, M. Stringer, and K. Hodges, 2012: An extratropical cyclone atlas: A tool for illustrating cyclone structure and evolution characteristics. *Bull. Amer. Meteor. Soc.*, **93**, 1497–1502, doi:10.1175/BAMS-D-11-00164.1.

Dee, D., and Coauthors, 2011: The ERA-Interim reanalysis: Configuration and performance of the data assimilation system. *Quart. J. Roy. Meteor. Soc.*, **137**, 553–597, doi:10.1002/qj.828.

Duncan, C., 1978: Baroclinic instability in a reversed shear flow. *Meteor. Mag.*, **107**, 17–23.

Forbes, G. S., and W. D. Lottes, 1985: Classification of mesoscale vortices in polar airstreams and the influence of the large-scale environment on their evolutions. *Tellus*, **37A**, 132–155, doi:10.1111/j.1600-0870.1985.tb00276.x.

Føre, I., J. E. Kristjánsson, Ø. Saetre, Ø. Breivik, B. Røsting, and M. Shapiro, 2011: The full life cycle of a polar low over the Norwegian Sea observed by three research aircraft flights. *Quart. J. Roy. Meteor. Soc.*, **137**, 1659–1673, doi:10.1002/qj.825.

Grønås, S., A. Foss, and M. Lystad, 1987: Numerical simulations of polar lows in the Norwegian Sea. *Tellus*, **39A**, 334–353, doi:10.1111/j.1600-0870.1987.tb00312.x.

Hewson, T., G. Graig, and C. Claud, 2000: Evolution and mesoscale structure of a polar low outbreak. *Quart. J. Roy. Meteor. Soc.*, **126**, 1031–1063, doi:10.1002/qj.49712656411.

Joly, A., and A. J. Thorpe, 1990: Frontal instability generated by tropospheric potential vorticity anomalies. *Quart. J. Roy. Meteor. Soc.*, **116**, 525–560, doi:10.1002/qj.49711649302.

Kolstad, E. W., 2006: A new climatology of favourable conditions for reverse-shear polar lows. *Tellus*, **58A**, 344–354, doi:10.1111/j.1600-0870.2006.00171.x.

Kristjánsson, J., and Coauthors, 2011: The Norwegian IPY–THORPEX. Polar lows and Arctic fronts during the 2008 Andøya campaign. *Bull. Amer. Meteor. Soc.*, **92**, 1443–1446, doi:10.1175/2011BAMS2901.1.

Laffineur, T., C. Claud, J.-P. Chaboureau, and G. Noer, 2014: Polar lows over the Nordic Seas: Improved representation in ERA-Interim compared to ERA-40 and the impact on downscaled simulations. *Mon. Wea. Rev.*, **142**, 2271–2289, doi:10.1175/MWR-D-13-00171.1.

Mallet, P.-E., C. Claud, C. Cassou, G. Noer, and K. Kodera, 2013: Polar lows over the Nordic and Labrador Seas: Synoptic circulation patterns and associations with North Atlantic–Europe wintertime weather regimes. *J. Geophys. Res. Atmos.*, **118**, 2455–2472, doi:10.1002/jgrd.50246.

McInnes, H., J. Kristiansen, J. E. Kristjánsson, and H. Schyberg, 2011: The role of horizontal resolution for polar low simulations. *Quart. J. Roy. Meteor. Soc.*, **137**, 1674–1687, doi:10.1002/qj.849.

Moore, R. W., and T. H. Vonder Haar, 2003: Diagnosis of a polar low warm core utilizing the Advanced Microwave Sounding Unit. *Wea. Forecasting*, **18**, 700–711, doi:10.1175/1520-0434(2003)018<0700:DOAPLW>2.0.CO;2.

Nielsen, N., 1997: An early-autumn polar low formation over the Norwegian Sea. *J. Geophys. Res.*, **102**, 13 955–13 973, doi:10.1029/97JD00281.

Noer, G., Ø. Saetra, T. Lien, and Y. Gusdal, 2011: A climatological study of polar lows in the Nordic Seas. *Quart. J. Roy. Meteor. Soc.*, **137**, 1762–1772, doi:10.1002/qj.846.

Nordeng, T. E., 1987: The effect of vertical and slantwise convection on the simulation of polar lows. *Tellus*, **39A**, 354–375, doi:10.1111/j.1600-0870.1987.tb00313.x.

——, and E. A. Rasmussen, 1992: A most beautiful polar low: A case study of a polar low development in the Bear Island region. *Tellus*, **44A**, 81–99, doi:10.1034/j.1600-0870.1992.00001.x.

——, and B. Røsting, 2011: A polar low named Vera: The use of potential vorticity diagnostics to assess its development. *Quart. J. Roy. Meteor. Soc.*, **137**, 1790–1803, doi:10.1002/qj.886.

Rasmussen, E. A., and J. Turner, 2003: *Polar Lows: Mesoscale Weather Systems in the Polar Regions*. Cambridge University Press, 612 pp.

Reed, R. J., and W. Blier, 1986: A case study of comma cloud development in the eastern Pacific. *Mon. Wea. Rev.*, **114**, 1681–1695, doi:10.1175/1520-0493(1986)114<1681:ACSOCC>2.0.CO;2.

——, and C. N. Duncan, 1987: Baroclinic instability as a mechanism for the serial development of polar lows: A case study. *Tellus*, **39A**, 376–384, doi:10.1111/j.1600-0870.1987.tb00314.x.

Sætra, Ø., Y. Gusdal, S. Eastwood, J. Debernard, P.-E. Isachesen, H. Schyberg, B. Furevik, and G. Noer, 2010: Scientific analysis plan (d3). Tech. Rep., Norwegian Meteorological Institute, 49 pp.

Sardie, J. M., and T. T. Warner, 1983: On the mechanism for the development of polar lows. *J. Atmos. Sci.*, **40**, 869–881, doi:10.1175/1520-0469(1983)040<0869:OTMFTD>2.0.CO;2.

Schär, C., and H. C. Davies, 1990: An instability of mature cold fronts. *J. Atmos. Sci.*, **47**, 929–950, doi:10.1175/1520-0469(1990)047<0929:AIOMCF>2.0.CO;2.

Terpstra, A., T. Spengler, and R. W. Moore, 2015: Idealised simulations of polar low development in an Arctic moist-baroclinic environment. *Quart. J. Roy. Meteor. Soc.*, **141**, 1987–1996, doi:10.1002/qj.2507.

Wilks, D. S., 2006: *Statistical Methods in the Atmospheric Sciences*. Academic Press, 627 pp.

Zahn, M., and H. von Storch, 2008: A long-term climatology of North Atlantic polar lows. *Geophys. Res. Lett.*, **35**, L22702, doi:10.1029/2008GL035769.

——, and ——, 2010: Decreased frequency of North Atlantic polar lows associated with future climate warming. *Nature*, **467**, 309–312, doi:10.1038/nature09388.

——, ——, and S. Bakan, 2008: Climate mode simulation of North Atlantic polar lows in a limited area model. *Tellus*, **60A**, 620–631, doi:10.1111/j.1600-0870.2008.00330.x.

Zappa, G., L. Shaffrey, and K. Hodges, 2014: Can polar lows be objectively identified and tracked in the ECMWF operational analysis and the ERA-Interim reanalysis? *Mon. Wea. Rev.*, **142**, 2596–2608, doi:10.1175/MWR-D-14-00064.1.